Nanolatticed architecture mitigates damage in shark eggcases

Rubayn Goh[1,], Scott P.O. Danielsen[2], Eric Schaible[3], Robert M. McMeeking[4], J. Herbert Waite[5,*]*

[1]Materials Department, University of California, Santa Barbara, CA 93106, USA.

[2]Thomas Lord Department of Mechanical Engineering and Materials Science, Duke University, Durham, NC 27708, USA.

[3]Advanced Light Source, Lawrence Berkeley National Laboratory, Berkeley, CA 94720, USA.

[4]Mechanical Engineering Department, University of California, Santa Barbara, CA 93106, USA.

[5]Department of Molecular, Cellular, and Developmental Biology, University of California, Santa Barbara, CA 93106, USA.

KEYWORDS: biological material, nanolattice, superlattice, mechanical metamaterial, nanoribbon, nanomechanics, nanostructure

ABSTRACT

Structural versatility and multifunctionality of biological materials have resulted in countless bioinspired strategies seeking to emulate the properties of nature. The nanostructured eggcase of swell sharks is one of the toughest permeable membranes known and thus, presents itself as a model system for materials where the conflicting properties — strength and porosity — are desirable. The eggcase possesses an intricately ordered structure that is designed to protect delicate embryos from the external environment while enabling respiratory and metabolic exchange, achieving a tactical balance between conflicting properties. Herein, structural analyses revealed an enabling nanolattice architecture that constitutes a Bouligand-like nanoribbon hierarchical assembly. Three distinct hierarchical architectural adaptations enhance eggcase survival: Bouligand-like organization for in-plane isotropic reinforcement, non-cylindrical nanoribbons maximize interfacial stress distribution, and highly ordered nanolattices enable permeability and lattice-governed toughening mechanisms. These discoveries provide fundamental insights for the improvement of multifunctional membranes, fiber-reinforced soft composites, and mechanical metamaterials.

TEXT

Nature has no equal in its ability to achieve multiple high-performance capabilities within the same material. Eggshells and eggcases are eloquent examples of multifunctional, protective structural materials.[1–3] Unlike the brittle eggshells of avian eggs, egg-laying elasmobranchs, such as sharks and skates, have evolved to produce leathery eggcases that allow the delicate embryos to survive in unrelentingly turbulent subtidal environments. The collagenous nature of elasmobranch eggcases has been well established by X-ray scattering and amino acid analyses.[4,5] Like tendon collagen, the ultrastructure of elasmobranch eggcases reveals an intricately ordered hierarchical structure spanning multiple length scales. However, the similarity to tendon collagen diverges at the nanoscale, where an exquisite permeable tetragonal network — resembling mechanical metamaterials — distinguishes the collagenous eggcase assembly.[4] Understanding the structural adaptations in these eggcases would provide insights into toughening strategies that would be of broad utility to the development of multifunctional soft composites,[6] ultrafiltration membranes,[7,8] and mechanical metamaterials.[9]

It is widely recognized that biochemical and ultrastructural adaptations play a crucial role in providing excellent energy absorbing properties and selective permeability mandatory for the survival of vulnerable embryos. Here, we describe how elaborate structural adaptations relate to mechanical properties in the eggcase of the swell shark, *Cephaloscyllium ventriosum*, an egg-laying (oviparous) elasmobranch endemic to the coast of central California.

Key to the ability of the swell shark eggcase to serve as a selective filtration membrane for gaseous and metabolic waste exchange is its inherent porosity. In practice, due to the loss of mass, porosities frequently lead to lower modulus and toughness – a trade-off that needs to be tactically balanced for permeable protective structures. Through a combination of microscopy and *in-situ* small angle X-ray scattering (SAXS) during tensile deformation,[10] we have identified structural adaptations and deformation mechanisms that are responsible for toughening the porous eggcase.

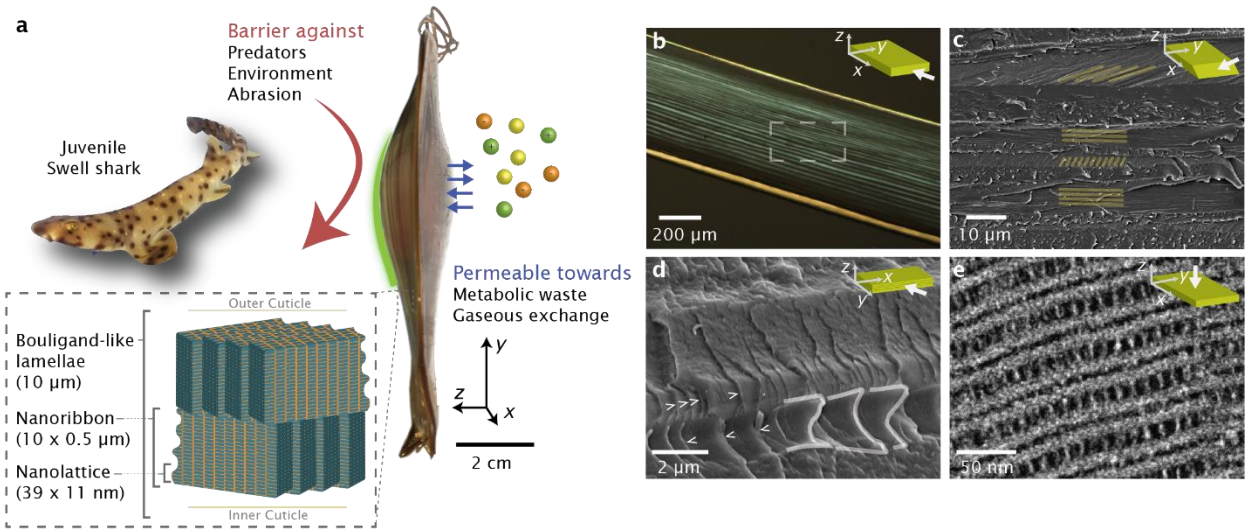

Figure 1. Hierarchical structure of the walls of the eggcase integrates both permeability and toughness. (a) Multifunctionality of eggcases ensures the survival of developing embryos. Inset illustrates the characteristic architectures of the eggcase with approximated dimensions. (b) Birefringence of the eggcase cross-section observed under polarized optical microscopy. The dashed box indicates the collagenous region of interest which constitutes the bulk of the eggcase and is seen under higher magnification with electron microscopy in panels (c) – (e). (c) Scanning electron microscopy (SEM) image of cryo-sectioned eggcase showing lamellae of unidirectional fibers with a ~30˚ – 60˚ rotation per layer. Direction of the fibers are highlighted. (d) SEM image of freeze-fractured eggcase emphasizing the non-cylindrical aspect of the fibers (nanoribbons). Nanoribbons are outlined to accentuate the non-symmetric and acylindrical aspect with chevrons pointing to the edge of the nanoribbons. (e) High magnification TEM image of the eggcase showing structured tetragonal pores within nanoribbons. Insets represent the approximate field of view.

Our structural analyses of eggcase using electron microscopy and SAXS revealed a hierarchically ordered structure from the micro- down to nanometer length scales (Fig. 1). At the microscale, the eggcase has a multi-ply lamellar organization with lamellae that are composed of single rows of unidirectional non-cylindrical fibers (nanoribbons). These nanoribbons have ~30˚ – 60˚ interlamellar rotation which gives rise to a Bouligand-like mesophase, providing the eggcase with in-plane isotropic mechanical reinforcement and crack bridging.[11,12] Strictly speaking, a Bouligand architecture has angular intervals with no discontinuities; therefore a ‘Bouligand-like’ description is more appropriate for the eggcase.[11,13] These nanoribbons have a height of ~3 – 10 µm, and estimates

based on the measurable edges of Figs. 1d and S2 suggest a nanoribbon thickness between ~0.15 – 0.3 µm. Because of the angle of view and the poorly defined edge boundaries, we would expect the actual thickness to vary from our estimates. Nonetheless, the approximated measurements would serve as a reference to the asymmetric aspect ratio of the nanoribbons. To avoid overstating our results, we assumed a nanoribbon thickness of 0.5 µm and compared it against cylindrical fibrils. In this case, the nanoribbon geometry provides an advantageous surface area to volume ratio that is 2.65 times larger than cylinders of equivalent volume (supplementary text). Ostensibly, the nanoribbons have been adapted to maximize stress distribution and energy transfer across the composite components.[14] At higher magnifications, ultrathin sections of the eggcase viewed under transmission electron microscopy (TEM) exhibited a highly ordered, pseudo-crystalline, tetragonal network that forms the nanoribbons.

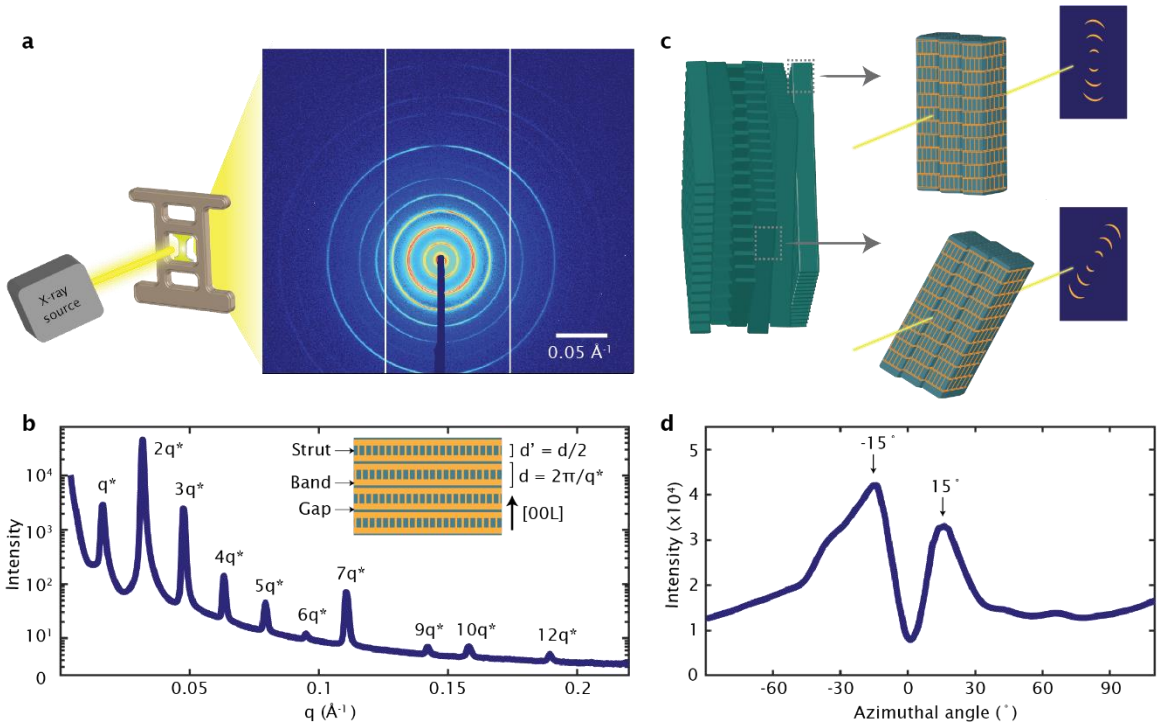

Figure 2. Synchrotron SAXS of the walls of the eggcase. (a) Experimental set up for *in-situ* SAXS during tensile deformation and the corresponding 2D SAXS of an unstrained sample. (b) Radial integration of 2D SAXS pattern of a representative sample with incident X-ray beam perpendicular to the xy-plane of the eggcase. Inset illustrates the superlattice morphology. (c) Illustration of nanolattice within a nanoribbon and the corresponding through-plane SAXS pattern. (d) Azimuthal integration of 2q* of a representative sample.

Through-plane SAXS reflections are consistent with a layered structure where q/q* = 1, 2, 3… with q* being the primary peak arising from the 39 nm spacings – corresponding with TEM observations (Figs. 2a, 2b). The exceptional order of the nanolattices was apparent in SAXS with reflections persistent up to the 12th order. The absence of SAXS peaks corresponding to the struts in the through-plane diffraction could be due to swelling of the struts or material around the struts influencing the electron density contrast, an increase in flexibility and mobility due to being in a hydrated state, and overshadowing by the q* peaks of significantly higher intensity. However, weak diffraction patterns arising from the diagonal planes are observed when the samples were rotated 90˚ (on-edge) with respect to the incident beam. The presence of these peaks supports the proposed body-centered tetragonal (BCT) symmetry that has been characterized in the dogfish eggcase (Fig. S3).[15] Intriguingly, the 2q* diffraction peak had a diffraction intensity greater than q* and the FFT of TEM images reflects a similar trend. To further investigate the origin of this, the q* and 2q* FFT peaks were masked and the corresponding inverse FFT overlayed on the TEM image (Fig. S4). The composite image emphasizes the remarkable regularity of the …ABCBAB… stacking. The nanolattice architecture bears a close resemblance to the proposed superlattice structure of charged block copolymers[16] and of oxygen-deficient perovskite derivatives,[17] wherein stacking of continuous and perforated layers alternates. To the best of our knowledge, a non-mineralized superlattice natural material has never been categorically identified and would serve as a pivotal model system for non-stochastic porous structures. Immediately obvious from the diffraction pattern is the absence of discretized nanoribbon orientation, unlike collagen fibers within the *Arapaima gigas* scales[11] or in uniaxially aligned collagen fibers in tendon.[18] Azimuthal integration of the 2q* diffraction peak indicated a continuous angular distribution of nanoribbons with a preferred orientation of ±15˚ with respect to the long axis (y-axis) of the eggcase (Figs. 2c, 2d).

To further investigate the mechanical characteristics and the role of the unique nanoarchitecture of the eggcase, we leveraged *in-situ* SAXS during tensile deformation. The walls of the eggcases were punched into dogbone-shaped samples, and the macroscopic strain along the gauge was measured by optical markers and tracked using a camera as the samples were elongated. Simultaneously, the evolution of texture was measured by X-ray scattering (Movie S1). Tensile characterization of the swell shark eggcases has revealed three distinct deformation regimes with transitions distinguished by a decrease in the stress-strain slope (modulus) of each regime. Analyses of the stress-strain curves of six eggcase samples indicated an initial modulus, measured by the slope of the 1st deformation

regime, of 107.9 ± 8.3 MPa and a strain to failure of 0.66 ± 0.04 (Fig. 3a); despite its porous nature and ~68% (w/w) water content. Comparatively, porous membranes made of polyvinylidene fluoride (PVDF) and polyether sulfone (PES) have lower elastic moduli of 10.5 and 8.7 MPa.[19]

The area under the stress-strain curves represents the maximum amount of strain energy per unit volume (work to failure, W_f) absorbed by the eggcases prior to failure. Subsequent integration of the area under the stress-strain curves obtained by our tensile characterization of the eggcase revealed an impressive W_f of 10.7 ± 1.0 MJ/m^3, approximately twice that of tendon which has a similar water content of ~62%.[20–22] With a measured density of 1.06 g/cm^3, the density-normalized W_f of 10 MJ/kg is 4 times greater than steel.[20] In comparison with recent innovations in strong and tough soft composites, the eggcase has an ultimate tensile strength, defined as the maximum stress prior to failure, of 25.4 ± 1.4 MPa exceeding that of fiber-reinforced soft composites (Fig. S5).[6] The exceptional mechanical properties of the eggcase along with its non-stochastic porosity would serve as a model system for future development of structurally robust thin membranes with high selectivity. Therefore, it will be beneficial to develop an understanding of the toughening and deformation process within the eggcase.

The non-monotonic stress-strain curve and distinct regimes with stepwise degradation of modulus of the eggcase, suggests a progressive failure of subcomponents within the architecture with well-defined fracture stress or yield points. By observing the diffraction patterns arising from the nanolattice during *in-situ* tensile deformation and corroboration by microscopy, we were able to determine the mechanisms involved in toughening of the eggcase. Analyses of the X-ray diffraction patterns indicate a cumulative engagement of fibers in the deformation of the eggcase (Fig. 3a). To glean additional insights into the strain distribution within the eggcase, and since q* arises from the 39 nm spacing observed in the nanolattice (Fig. 2b), the intensity of line profiles along 0˚, 45˚, and 90˚ were integrated across the 2D SAXS of a representative sample at each strain interval. The corresponding *d-spacings* of the strained samples were then approximated by the peak position of a Voigt-fitted q*. Because the nanolattices are aligned within nanoribbons (Fig 2c), the nanoribbon strain could thus be approximated by the change in *d-spacing* over the original *d-spacing* or rewritten as $(q_0^*/q^*) - 1$, where q_0^* is q* of the unstrained state. The nanoribbon strains were then plotted against sample strain to elucidate the general response of the nanoribbons at different angles (Fig. 3b).

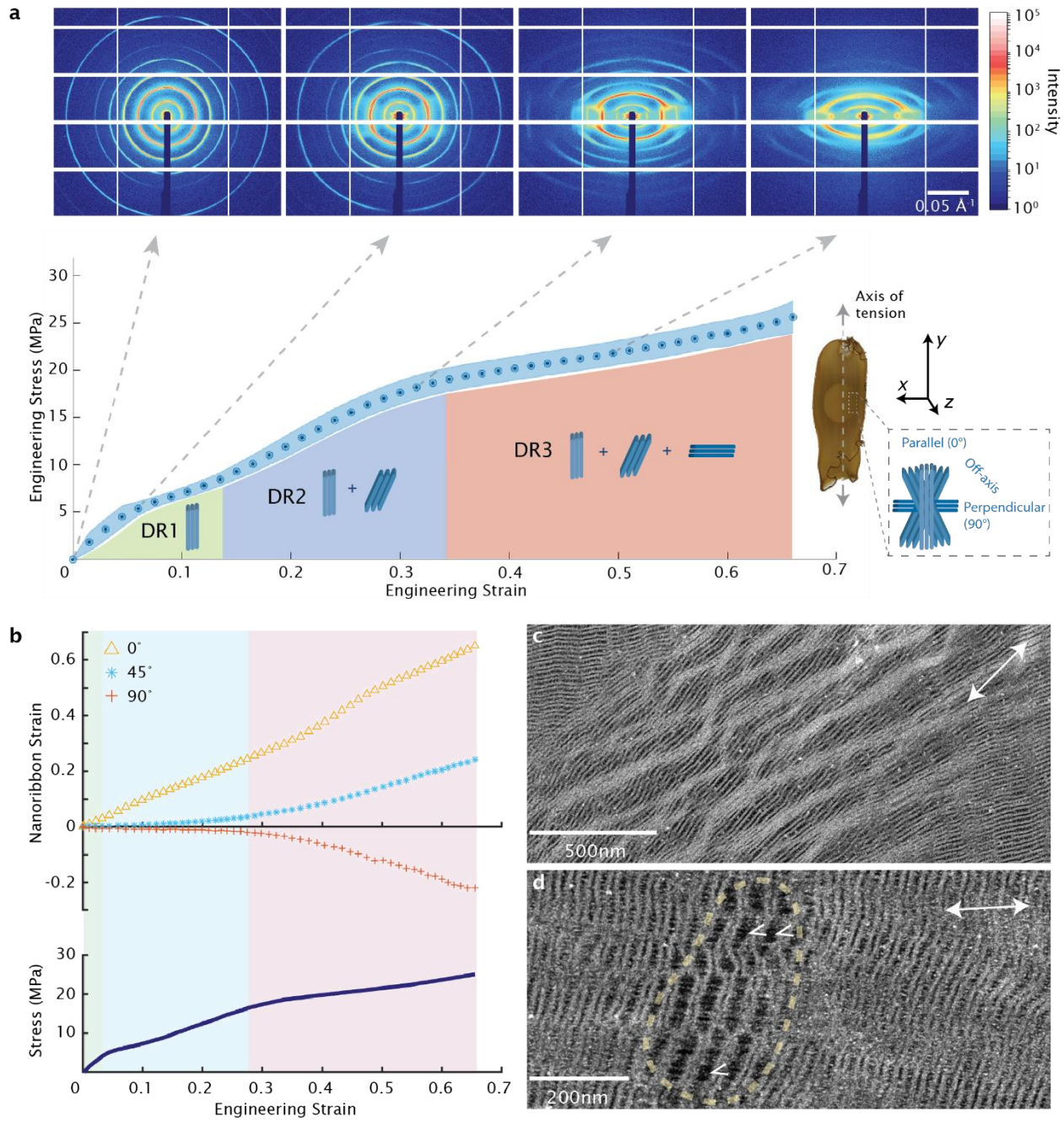

Figure 3. Elucidation of deformation mechanisms using i*n-situ* SAXS during tensile deformation and TEM. (a) Stress-strain curve of swell shark eggcase with three distinct deformation regimes (DR) and corresponding SAXS patterns at ε = 0%, 5.8%, 31%, and 50%. Inset illustrates the stress axis with respect to the eggcase and nanoribbon orientations. Data is the mean ± s.d. (shaded region) of six experiments. (b) Nanoribbon strain along 0˚, 45˚ and 90˚ of a representative sample plotted against sample strain. TEM of eggcase strained to 25% strain showing (c) shear

bands and rotation of nanolattices and (d) nucleation of crack encircled by dashed line as well as fracturing of struts indicated by chevrons. Stress axes indicated by arrows.

The 1st deformation regime involved elongation of the nanoribbons parallel to the stress axis while the 2nd regime then engaged the off-axis fibers in the deformation process. As the nanoribbons deformed in the 1st and 2nd regimes, a gradual decrease in scattering intensity and order of nanoribbons parallel to the stress axis occurred. Accordingly, the onset of the 2nd deformation regime and the consequent decrease in modulus coincided with the observations of significant reorientation and uniform shear banding in samples that were chemically fixed while strained to the 2nd regime (Fig. 3c). In this case, both elastic and non-elastic structural deformations were arrested by chemical fixatives that extensively crosslinked the eggcase at the molecular level. TEM micrographs of the onset of shear bands suggest that failure primarily happened along the planes of lowest density – along the struts and gap region. In all cases, the long axes of the shear bands were oriented along the macroscopic tensile axis. Consideration of the formation of shear bands within a simplified anisotropic model[23] agrees with the observed directions of the shear bands and supports the eventual formation of the diamond-shaped damage zones (Fig. S6) seen in the egg case (supplementary text). Such features resemble the toughening mechanism seen in metallic glass composites that facilitates uniform nucleation and distribution of shear bands. This prevents the formation of critical strain localization, leading to an overall increase in ductility.[24] Additionally, lattice reorientation of up to 65˚ was also observed with weak planes preferentially reoriented parallel to the stress axis, facilitating shear deformation along susceptible planes. Reorientations were independent of nanoribbon orientation as seen by isolated islands of reoriented nanolattices while the reorientation preference is indicative of a deformation mechanism that is governed by lattice asymmetry (Fig. S6). Consequent of the geometric softening mechanisms, higher strains could be accommodated by the nanoribbons thereby toughening the eggcase.

In the 3rd regime, nanoribbons perpendicular to the stress axis shortened due to Poisson's effect arising from strain perpendicular to the nanoribbon axis. Simultaneous compressive forces from Poisson's contraction of adjacent lamellae could additionally contribute to the effective shortening of the nanoribbons.[11] At the same time, an increase in diffraction intensity parallel to the stress axis was observed implying an increase in nanolattice alignment. The increase in scattering intensity at q* was significantly more than at 2q*, suggesting a disruption of the hierarchical superlattice and is supported by the increasingly disordered structure seen by TEM (Figs. S7, S8). Conversely, the

intensity ratio of the off-axis nanolattices remains consistent with the initial observation where 2q* is greater than q*, pointing to the conservation of the superlattice symmetry along the off-axis orientation (Fig. S7).

Examining the strain of nanoribbons parallel to the stress axis indicates a deformation rate that was similar to the macroscopic strain throughout all three regimes and to a nanoribbon strain of 76 ± 6.6%. The discrepancy between nanoribbon and macroscopic strain was presumed to be due to variation of strain across the sample caused by non-homogenous thickness. The comparable deformation implies that the strain in the nanoribbons parallel to the stress axis was continuous across the eggcase unlike collagenous tendons[18,25] and fish scales.[11] The ability of the nanoribbons to sustain high strains prior to failure, exceeding collagen fibril strain by ~1800%,[18,25] can be attributed to the tetragonal architecture within the nanoribbon. Besides lattice-governed shear banding and reorientation, the presence of porosities minimize constraints by the surrounding materials during deformation while acting as stress concentrators that provide nucleation sites for crack propagation (Fig. 3d).[26] The struts act as effective crack bridges and given the nanoscale architecture of the lattice, exploitation of size-dependent material strengthening effects at the nanometer length-scale would, in principle, improve flaw insensitivity as well.[9,27–29]

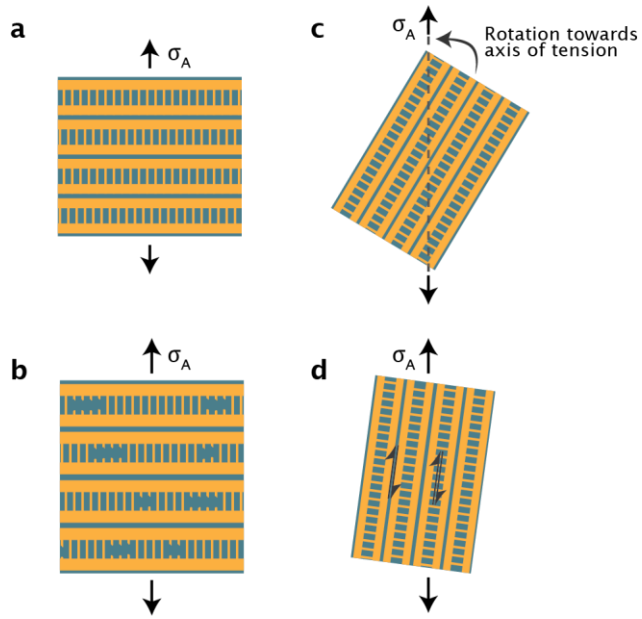

Figure 4. Deformation mechanisms seen in the nanolattice architecture from *in-situ* SAXS during tensile deformation and TEM. (a) Distortion of nanolattice architecture, (b) fracturing of struts, (c) rotation, and (d) nucleation of shear bands along weak planes with σ_A being the applied stress.

In conclusion, swell shark eggcases showcase extensive structural adaptions and unique deformation processes in a highly intricate hierarchical architecture. In our work, we have identified a Bouligand-like architecture that provides in-plane quasi-isotropic mechanical reinforcement, acylindrical nanoribbons optimized for effective stress distribution, and an exceptionally ordered nanolattice architecture that gives rise to lattice-governed toughening mechanisms while permitting selective permeability. The most notable discoveries are a cumulative deformation mechanism that involves a stepwise engagement of nanoribbons of different orientations, and lattice-governed toughening mechanisms that facilitates plasticity (Fig. 4). The asymmetry and reorientation of the nanolattice make possible the uniform formation of multiple non-critical shear bands, as seen in the toughening of metallic glass composites.[24] Disruption of the superlattice symmetry only at high strains suggests a critical yield-point of a substructure within the lattice. Although impossible to resolve the exact substructure at this time, the stepwise deformation of the nanolattice serves as an effective toughening mechanism by giving rise to hidden lengths when disrupted, a common strategy in biological materials[30] and novel synthetic elastomers.[31] Despite a decrease in stiffness at higher strains due to geometric softening effects, the combination of cumulative nanoribbon engagement and lattice-governed toughening mechanisms gives rise to strain hardening and a high strain to failure. Given the impressive toughness despite porosity and high water content, the swell shark eggcase merits further scrutiny and offers timely inspiration for improved multifunctional membranes and mechanical metamaterials. These discoveries will also serve as the cornerstone and inspiration for future work on nanolattice protein self-assembly.

ASSOCIATED CONTENT

Movie S1: In-situ SAXS during tensile deformation of the swell shark eggcase.

Supplementary: Experimental details, supporting discussion of observed structural adaptations, Ashby plots, interpretation of SAXS data as a BCT, FFT overlay, TEM images and FFT analysis of strained eggcases, and integrated SAXS intensity along the stress axis across the deformation regimes.

AUTHOR INFORMATION

Corresponding Authors

Rubayn Goh — Materials Department, University of California, Santa Barbara, CA 93106, USA.

https://orcid.org/0000-0001-8333-8143

Email: rgoh@ucsb.edu

J. Herbert Waite — Department of Molecular, Cellular, and Developmental Biology, University of California, Santa Barbara, CA 93106, USA. https://orcid.org/0000-0003-4683-7386

Email: hwaite@ucsb.edu

Author Contributions

The manuscript was written through contributions of all authors. All authors have given approval to the final version of the manuscript.

ACKNOWLEDGMENT

We thank R. Segalman, M. Valentine, A. Kossa, Y. Li, A. Miserez, A. Patterson, J. Booth, K.S. Qwah, and B. Tan for the productive discussions, C. Pierre, C. Orsini and S. Simon from UCSB Marine Operations and The REEF for the collection and generous contribution of the eggcases, and A. Taylor for his technical assistance. The research reported here was supported in part by the National Science Foundation (NSF) Materials Research Science and Engineering Center (MRSEC) at UC Santa Barbara (NSF DMR 1720256) through IRG-3. Individual fellowship support of R.G. was provided by Agency for Science, Technology and Research (A*STAR). X-ray scattering was performed at the Advanced Light Source, a DOE Office of Science User Facility (DE-AC02-05CH11231; beamline 7.3.3). We acknowledge the use of the shared facilities of the NSF MRSEC (DMR 1720256), the NRI-MCDB Microscopy Facility, and the research facilities within California NanoSystems Institute, supported by UC Santa Barbara, and the UC Office of the President at UC, Santa Barbara.

ABBREVIATIONS

W_f, work to failure; SAXS, small angle X-ray scattering; TEM, transmission electron microscopy; FFT, fast fourier transform; BCT; body-centered tetragonal; DR; deformation regime

REFERENCES

(1) Chang, Y.; Chen, P.-Y. Hierarchical Structure and Mechanical Properties of Snake (Naja Atra) and Turtle (Ocadia Sinensis) Eggshells. *Acta Biomaterialia* **2016**, *31*, 33–49.

(2) Hahn, E. N.; Sherman, V. R.; Pissarenko, A.; Rohrbach, S. D.; Fernandes, D. J.; Meyers, M. A. Nature's Technical Ceramic: The Avian Eggshell. *J. R. Soc. Interface.* **2017**, *14* (126), 20160804.

(3) Miserez, A.; Wasko, S. S.; Carpenter, C. F.; Waite, J. H. Non-Entropic and Reversible Long-Range Deformation of an Encapsulating Bioelastomer. *Nature Mater* **2009**, *8* (11), 910–916.

(4) Knight, D. P.; Feng, D.; Stewart, M. Structure and Function of the Salachian Egg Case. *Biological Reviews* **1996**, *71* (1), 81–111.

(5) Knight, D. P.; Hunt, S. Fibril Structure of Collagen in Egg Capsule of Dogfish. *Nature* **1974**, *249* (5455), 379–380.

(6) King, D. R.; Sun, T. L.; Huang, Y.; Kurokawa, T.; Nonoyama, T.; Crosby, A. J.; Gong, J. P. Extremely Tough Composites from Fabric Reinforced Polyampholyte Hydrogels. *Mater. Horiz.* **2015**, *2* (6), 584–591.

(7) Yan, L.; Li, Y. S.; Xiang, C. B.; Xianda, S. Effect of Nano-Sized Al2O3-Particle Addition on PVDF Ultrafiltration Membrane Performance. *Journal of Membrane Science* **2006**, *276* (1), 162–167.

(8) Landsman, M. R.; Sujanani, R.; Brodfuehrer, S. H.; Cooper, C. M.; Darr, A. G.; Davis, R. J.; Kim, K.; Kum, S.; Nalley, L. K.; Nomaan, S. M.; Oden, C. P.; Paspureddi, A.; Reimund, K. K.; Rowles, L. S.; Yeo, S.; Lawler, D. F.; Freeman, B. D.; Katz, L. E. Water Treatment: Are Membranes the Panacea? *Annu. Rev. Chem. Biomol. Eng.* **2020**, *11* (1), 559–585.

(9) Bauer, J.; Meza, L. R.; Schaedler, T. A.; Schwaiger, R.; Zheng, X.; Valdevit, L. Nanolattices: An Emerging Class of Mechanical Metamaterials. *Advanced Materials* **2017**, *29* (40), 1701850.

(10) Hexemer, A.; Bras, W.; Glossinger, J.; Schaible, E.; Gann, E.; Kirian, R.; MacDowell, A.; Church, M.; Rude, B.; Padmore, H. A SAXS/WAXS/GISAXS Beamline with Multilayer Monochromator. *J. Phys.: Conf. Ser.* **2010**, *247*, 012007.

(11) Zimmermann, E. A.; Gludovatz, B.; Schaible, E.; Dave, N. K. N.; Yang, W.; Meyers, M. A.; Ritchie, R. O. Mechanical Adaptability of the Bouligand-Type Structure in Natural Dermal Armour. *Nat Commun* **2013**, *4* (1), 2634.

(12) Quan, H.; Yang, W.; Schaible, E.; Ritchie, R. O.; Meyers, M. A. Novel Defense Mechanisms in the Armor of the Scales of the "Living Fossil" Coelacanth Fish. *Advanced Functional Materials* **2018**, *28* (46), 1804237.

(13) Bouligand, Y. Twisted Fibrous Arrangements in Biological Materials and Cholesteric Mesophases. *Tissue and Cell* **1972**, *4* (2), 189–217.

(14) Crosby, A. J.; Lee, J.-Y. Polymer Nanocomposites: The "Nano" Effect on Mechanical Properties. *Polymer Reviews* **2007**, *47* (2), 217–229.

(15) Knupp, C.; Chew, M.; Morris, E.; Squire, J. Three-Dimensional Reconstruction of a Collagen IV Analogue in the Dogfish Egg Case Wall. *Journal of Structural Biology* **1996**, *117* (3), 209–221.

(16) Shim, J.; Bates, F. S.; Lodge, T. P. Superlattice by Charged Block Copolymer Self-Assembly. *Nature Communications* **2019**, *10* (1), 2108.

(17) Jeen, H.; Choi, W. S.; Biegalski, M. D.; Folkman, C. M.; Tung, I.-C.; Fong, D. D.; Freeland, J. W.; Shin, D.; Ohta, H.; Chisholm, M. F.; Lee, H. N. Reversible Redox Reactions in an Epitaxially Stabilized SrCoOx Oxygen Sponge. *Nature Materials* **2013**, *12* (11), 1057–1063.

(18) Fratzl, P.; Misof, K.; Zizak, I.; Rapp, G.; Amenitsch, H.; Bernstorff, S. Fibrillar Structure and Mechanical Properties of Collagen. *Journal of Structural Biology* **1998**, *122* (1), 119–122.

(19) Acarer, S.; Pir, İ.; Tüfekci, M.; Türkoğlu Demirkol, G.; Tüfekci, N. Manufacturing and Characterisation of Polymeric Membranes for Water Treatment and Numerical Investigation of Mechanics of Nanocomposite Membranes. *Polymers* **2021**, *13* (10), 1661.

(20) Denny, M. W. Properties of Biological Materials. In *Biology and the Mechanics of the Wave-Swept Environment*; Princeton University Press, 1988; pp 176–194.

(21) Bailey, A. J.; Macmillan, J.; Shrewry, P. R.; Tatham, A. S.; Gosline, J.; Lillie, M.; Carrington, E.; Guerette, P.; Ortlepp, C.; Savage, K. Elastic Proteins: Biological Roles and Mechanical Properties. *Philosophical Transactions of the Royal Society of London. Series B: Biological Sciences* **2002**, *357* (1418), 121–132.

(22) Fullerton, G. D.; Amurao, M. R. Evidence That Collagen and Tendon Have Monolayer Water Coverage in the Native State. *Cell Biology International* **2006**, *30* (1), 56–65.

(23) Nizolek, T. J.; Pollock, T. M.; McMeeking, R. M. Kink Band and Shear Band Localization in Anisotropic Perfectly Plastic Solids. *Journal of the Mechanics and Physics of Solids* **2021**, *146*, 104183.

(24) Albe, K.; Ritter, Y.; Şopu, D. Enhancing the Plasticity of Metallic Glasses: Shear Band Formation, Nanocomposites and Nanoglasses Investigated by Molecular Dynamics Simulations. *Mechanics of Materials* **2013**, *67*, 94–103.

(25) Sasaki, N.; Odajima, S. Elongation Mechanism of Collagen Fibrils and Force-Strain Relations of Tendon at Each Level of Structural Hierarchy. *Journal of Biomechanics* **1996**, *29* (9), 1131–1136.

(26) Notario, B.; Pinto, J.; Rodriguez-Perez, M. A. Nanoporous Polymeric Materials: A New Class of Materials with Enhanced Properties. *Progress in Materials Science* **2016**, *78–79*, 93–139.

(27) Bauer, J.; Schroer, A.; Schwaiger, R.; Kraft, O. Approaching Theoretical Strength in Glassy Carbon Nanolattices. *Nature Mater* **2016**, *15* (4), 438–443.

(28) Zhao, X. Designing Toughness and Strength for Soft Materials. *Proc Natl Acad Sci USA* **2017**, *114* (31), 8138–8140.

(29) Gao, H.; Ji, B.; Jager, I. L.; Arzt, E.; Fratzl, P. Materials Become Insensitive to Flaws at Nanoscale: Lessons from Nature. *Proceedings of the National Academy of Sciences* **2003**, *100* (10), 5597–5600.

(30) Ritchie, R. O. The Conflicts between Strength and Toughness. *Nature Mater* **2011**, *10* (11), 817–822.

(31) Brown, C. L.; Craig, S. L. Molecular Engineering of Mechanophore Activity for Stress-Responsive Polymeric Materials. *Chem. Sci.* **1393**, *6* (4), 2158–2165.

TOC Graphic

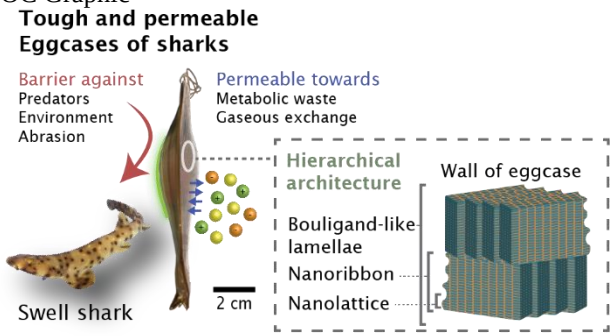
Tough and permeable
Eggcases of sharks
Barrier against
Predators
Environment
Abrasion
Permeable towards
Metabolic waste
Gaseous exchange
Hierarchical architecture
Wall of eggcase
Bouligand-like lamellae
Nanoribbon
Nanolattice
2 cm
Swell shark